JOURNAL OF SPACECRAFT AND ROCKETS
Vol. 31, No. 6, November–December 1994

Fluid Dynamics Within a Rotating Bioreactor in Space and Earth Environments

Yow-Min D. Tsao*
KRUG Life Sciences, Houston, Texas 77058
Ernest Boyd†
Mankato State University, Mankato, Minnesota 56001
and
David A. Wolf‡ and Glenn Spaulding§
NASA Johnson Space Center, Houston, Texas 77058

We recently developed a mathematical model to characterize cell-medium interactions within a Couette-flow bioreactor (concentric independent rotating vessel). Such models will be used to refine the conditions in bioreactors to achieve optimal cell growth. Numerical simulations and space-flight experiments have been conducted to test the model. Anchorage-dependent mammalian cell aggregates on the microcarrier beads in dynamic flow environments were simulated by the trajectories of particles in the flowfield. The flowfield for the circulation of the culturing medium was modeled by the Navier-Stokes equations. The forces on a particle were assumed to be drag from fluid circulation, buoyancy from gravitational fields, and centrifugal forces from the rotation of the vessel. We first solved the momentum equations for the steady-state fluid flow and then the equations for the motion of a particle. Results obtained from this study indicated that in unit gravity the bioreactor would simulate primary microgravity trajectories of particles and migration times. However, rotating the bioreactor under the influence of gravity produces a significant component of particle motion and associated shear stress not found in a microgravity environment. Moreover, the total force per unit of cross-sectional area on a particle in microgravity was significantly smaller than the calculated value in unit gravity. Experimental results from space flight support the numerical simulations.

Nomenclature

d = diameter of a microcarrier bead, μm
g = gravity acceleration, cm/s^2
m = $\rho_p \pi d^3/6$
Re_i = inner-cylinder Reynolds number
Re_o = outer-cylinder Reynolds number
r = radial component
r_i = radius of inner cylinder, cm
r_o = radius of outer cylinder, cm
u = radial component of velocity, cm/s
v = angular component of velocity, cm/s
w = axial component of velocity, cm/s
z = axial component
α = $3\pi d\mu$
β = $(\rho_p - \rho_s)\pi d^3/6$
$\Delta\omega$ = differential rotating rate, rpm
θ = angular component
μ = viscosity, g/cm·s
ρ_p = density of microcarrier bead, g/cm^3
ρ_s = density of the culture medium, g/cm^3
ω_i = rotation rate of inner cylinder, rpm
ω_0 = rotation rate of outer cylinder, rpm

Introduction

Background

THE Couette-flow bioreactor described here was developed for culturing mammalian cells. The system was designed to provide a uniform low-shear environment with controllable shear levels. This allows the suspension of anchorage-dependent cells in a low-gravity (low-shear) three-dimensional favorable culture environment. A major design requirement was the need to suspend cells and cell aggregates on microcarrier beads (emulated as particles) with continuous perfusion while maintaining in the environment the minimum shear possible in the presence of gravity. The design provided sufficient circulation for adequate oxygenation and mass transfer of nutrients to the cells through mechanical methods. Such a rotational suspension system requires that inherent mechanical agitation mechanisms be minimized. Strong shear effects in the system could damage delicate cells, and are hypothesized to degrade the formation of three-dimensional tissue-like structures.[1] Microgravity is believed to provide the best environment[2,3] for optimizing the assembly of tissues from elementary cells and substrates. Partially simulating microgravity hydrodynamics, the NASA rotating-wall perfusion vessel has shown excellent performance. In this study, we sought to characterize the hydrodynamics of these vessels in an effort to predict whether further improvements could be realized in space, where the residual gravity-induced stresses are absent.

Numerous studies have been conducted to examine the effects of hydrodynamic forces on cellular growth and damage. Cells growing on glass slides or cover slips exhibited no shear damage when subjected to fluid shear stresses from 6.5 to 30 dyne/cm^2. However, the laminar-flow two-dimensional environment was not imposed upon cells with sensitive cytoplasmic extensions or cells developing into tissue-like three-dimensional structures.

Stathopoulos and Hellums[4] reported that morphological changes in human embryonic kidney cells occurred at a shear force of 2.6 dyne/cm^2; significant damage to the cells was observed at 10 dyne/cm^2. Other studies have attempted to evaluate the damage created in three-dimensional vessels which were vigorously agitated in an effort to overcome unit-gravity particle sedimentation. Reports from Croughan's laboratory[5,6] showed that in spinner vessels with magnetic stirrers, cell growth was correlated with a time-averaged shear rate proportional to the tip speed of the impeller.

Received June 27, 1992; revision received Jan. 21, 1994; accepted for publication Jan. 22, 1994.

*Senior Engineer, Section Supervisor, Biotechnology Facility, 1290 Hercules Drive, Suite 120.
†Associate Professor, Department of Mathematics.
‡Astronaut, Astronaut Office.
§Medical Officer-Immunology, Program Manager-Biotechnology, Medical Sciences Division.

They concluded that there was no detrimental hydrodynamic effects on the growth of Vero cells in a traditional 250-ml spinner vessel with a rotation rate up to 60 rpm. Moreover, they reported optimal growth of FS-4 cells in 125-ml vessels at 35 rpm. Cell growth, correlated to the Kolmogorov eddy length in an analysis of turbulence, was modeled as well. It has been reported that "for complete off-bottom suspension of microcarriers (in unit gravity), virtually all stirred vessels must be agitated at the turbulent regime."

Cherry and Papoutsakis[7] estimated the magnitude of various hydrodynamic effects on cells with microcarriers in agitated culture reactors. The maximum shear stress on a particle sinking through a liquid at settling velocity was calculated to be 0.07 dyne/cm^2. The maximum shear stress in a typical stirred vessel would be 5 dyne/cm^2 in the boundary layer along the wall. Cherry and Papoutsakis[8] discussed a model of the growth correlated with collisions of a particle with the impeller and the vessel walls. Studies by Goodwin and Wolf[9] using BHK-21 cells in the rotating-wall perfusion vessel suggest that shear stress of 1 dyne/cm^2 would directly influence cell growth rates and the aggregation of cells on the beads into three-dimensional complexes. These studies, however, did not include analyses of the total force on a particle as a complete dynamical system in three dimensions. Hence, complete simulations of the full dynamic system and the hydrodynamic forces, with estimations of the frequency of collisions with the vessel walls, become essential. At the same time, previous studies indicate that turbulence with eddies on the same scale as the diameter of a particle can damage cells. Therefore, the design of the vessel should attempt to minimize turbulence.

Rotating culture vessels have been designed for use in microgravity and unit gravity.[10] These vessels minimize agitation and turbulence, reduce the total fluid shear stress,[11] provide a homogeneous environment for the cells, and have had significant success in developing high-fidelity tissue assemblies for clinical research. The purpose of the study reported here was to develop a numerical model of the culture vessel to provide insight into why cultured cells assembled into high-fidelity tissue. The model assumes the movement of cell aggregates to be particle trajectories, and allows calculations of the total force on particles suspended in the vessel. The intent of the model was to simulate both microgravity and unit-gravity cell suspensions in order to elucidate precise physical mechanisms that would exploit microgravity conditions for further enhanced tissue culture. This quantitative study also provides information for improving design and operation of space-based bioreactors.

Description of the Concentric Rotating Bioreactor and Analysis of Hydrodynamic Forces

The bioreactor modeled here was designed to provide a Couette flowfield with nearly uniform shear stress throughout the vessel. The vessel consists of two concentric cylinders, both 11 cm long, with the outer cylinder having a radius of $r_o = 4.0$ cm and rotating at ω_o rpm, while the inner cylinder has a radius of $r_i = 2.86$ cm and rotates in the same direction at ω_i rpm. The end walls of the vessel are fixed with the outer cylinder and rotate with it. The gap of 1.14 cm between the cylinders was completely filled with culture medium into which particles (models of aggregates of cells) and microcarrier beads were introduced. Figure 1 provides a schematic representation of the vessel. Cylindrical coordinates (r, θ, z) were used to indicate positions within the vessel, where r is the radial component measured outward relative to the cylinders, with $r_i < r < r_o$, θ is the angular component measured positively in the direction of rotation of the two cylinders, and z is the axial component oriented horizontally in a gravitational field with $0 < z < 11$ cm.

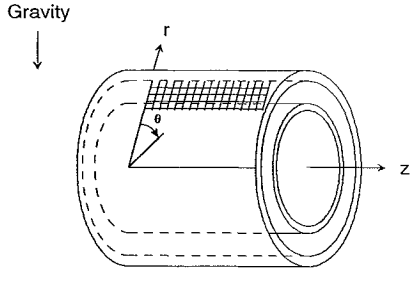

Fig. 1 Schematic of the rotating bioreactor.

Assumptions for this mathematical simulation were as follows:

1) The culturing medium, or substrate, was a Newtonian fluid with a constant density $\rho_s = 1.02$ g/cm^3 and a constant viscosity $\mu = 0.0097$ g/cm·s.

2) Particles were spherical in shape with a diameter $d = 175\ \mu$m and a density $\rho_p = 1.04$ g/cm^3, did not interact with one another, and did not affect the flow of the culturing medium.

3) The flow of the culturing medium caused by the rotation of the concentric cylinders was a laminar, axially symmetric Couette flow governed by the Navier-Stokes equation.

4) The forces acting on a particle were drag from the fluid's circulation, buoyancy from the gravitational force relative to the difference between the densities of a particle and the fluid, and centrifugal force from the rotation of the vessel. The numerical values in assumptions 1 and 2 correspond to anticipated early stages of cellular growth in the bioreactor using Cytodex-3 microcarriers in a standard medium with 10% fetal calf serum.

Let u, v, and w represent the radial, circumferential, and axial velocity, respectively, components of the flowfield. The rates of rotation of the cylinders were limited to a range in which u, v, and w were large enough to suspend particles in unit gravity and provide adequate mixing, but small enough to prevent turbulence. The unique advantage of this concentric rotating bioreactor was that the fluid shear force created by the differential rate of rotation of the two cylinders would be more uniform and controllable, and thereby providing a better-controlled environment for understanding the effects of fluid shear on three-dimensional cell culture.

When there is a steady flow of constant density around a submerged spherical bead, the fluid will exert a force on the solid bead surface. This force may be categorized in two parts: the background force and the kinetic force. To describe the background force, the flowfield between two concentric rotating cylinders is used. The velocity profile can be derived by the balance of the centrifugal force, pressure gradient force, and viscous force. The background shear stress can be estimated from the velocity gradient, and we projected this force onto the plane of characteristic area for convenience of comparison with the kinetic force. The kinetic force points in the same direction as the approach velocity and is defined as a product of a characteristic area, the kinetic energy, and the drag coefficient. This force can also be called the drag force. In our calculations, we use the terminal velocity for the steady-state fall of a spherical bead as the approach velocity. Figure 2 shows the sum of the background shear force at a differential rotating rate of 6 rpm and the drag force (kinetic force) in unit gravity on particles of different sizes in the bioreactor. The total force experienced by a 175-μm particle was about 0.6 dyne/cm^2. When the approach flow velocity to a particle was kept constant, smaller particles experienced stronger viscous effect. Therefore, at the beginning of cell culturing the cell would experience a stronger drag force per unit area from the same approaching flow velocity. Hence, minimizing the flow velocity in the early stages of the cell culturing becomes important. This represents an ideal use of microgravity, since during the early stages of the cell culturing there is already a sufficient supply of oxygen and nutrients so that with the absence of sedimentation the bioreactor does not need to be rotated at all, i.e., a quiescent environment can be maintained while the initial aggregates of cells and microcarriers become established.

The results shown in Fig. 2 did not take into account the dynamical motion of particles. Hence, they may overestimate the total force actually experienced by particles. Therefore, a mathematical model of the dynamics of a particle motion was developed to obtain detailed information on particle flow patterns, the particle trajectory, and the total force on a particle.

Dynamical Model

Assume (u, v, w) represent the (radial, circumferential, axial) components of the velocity of the flow field as functions of time t.

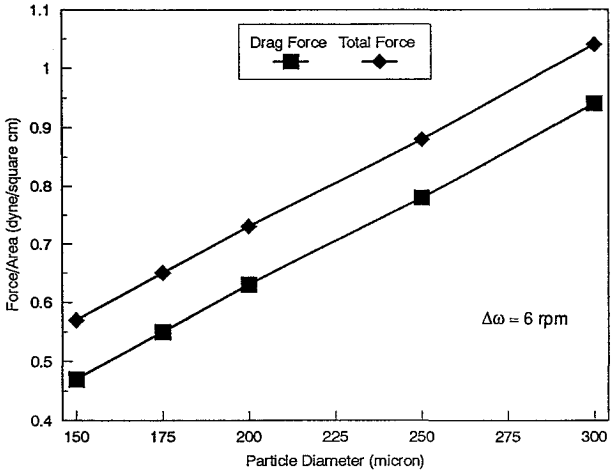

Fig. 2 Hydrodynamic forces acting on particles in unit gravity.

Then the Navier-Stokes equations for the flow field are[12]

$$\frac{1}{r}\frac{\partial(ru)}{\partial r} + \frac{\partial w}{\partial z} = 0 \tag{1}$$

$$\frac{Du}{Dt} - \frac{v^2}{r} = -\frac{1}{\rho_s}\frac{\partial P}{\partial r} + \frac{\mu}{\rho_s}\left(\nabla^2 u - \frac{u}{r^2}\right) \tag{2}$$

$$\frac{Dv}{Dt} + \frac{uv}{r} = \frac{\mu}{\rho_s}\left(\nabla^2 v - \frac{v}{r^2}\right) \tag{3}$$

$$\frac{Dw}{Dt} = -\frac{1}{\rho_s}\frac{\partial p}{\partial z} + \frac{\mu}{\rho_s}\nabla^2 w \tag{4}$$

where

$$\frac{D}{Dt} = \frac{\partial}{\partial t} + u\frac{\partial}{\partial r} + w\frac{\partial}{\partial z}$$

$$\nabla^2 = \frac{1}{r}\frac{\partial}{\partial r}\left(r\frac{\partial}{\partial r}\right) + \frac{\partial^2}{\partial z^2}$$

and P is the fluid pressure measured in dyne/cm^2. The boundary conditions for the flowfield were the standard constraints of no slip and no penetration.

The momentum equations for a trajectory of a particle contain terms for the forces of Stokes drag, gravitational buoyancy, and centrifugal effect.[13] If (r, θ, z) represent the position of a particle at time t, then the equations of motion of a particle are

$$m\frac{d^2r}{dt^2} = -\alpha\left(\frac{dr}{dt} - u\right) - \beta g\cos\theta + \beta r\left(\frac{d\theta}{dt}\right)^2 \tag{5}$$

$$mr\frac{d^2\theta}{dt^2} = -\alpha\left(r\frac{d\theta}{dt} - v\right) - \beta g\sin\theta \tag{6}$$

$$m\frac{d^2z}{dt^2} = -\alpha\left(\frac{dz}{dt} - w\right) \tag{7}$$

In this study, the initial conditions for a particle at $t = 0$ were taken to be $r = 3$ cm, $\theta = 0, z = 1, 2.5, 4, 7, 8.5$, or 10 cm, and the derivatives were all set equal to zero.

Preliminary studies consisted of three trials using different rotation speeds ω_i and ω_o for the inner and outer-cylinders. The rotation rates are listed in Table 1. Ranges were chosen based on current operationally practical usage rates with the intent of extrapolating the results to microgravity for comparison of values derived from the model with the experimental results derived from U.S. Space Shuttle flights. The flowfield in this study was designed to avoid instability from the centrifuge effect. The inner-cylinder Reynolds number (Re_i) ranged from 850 to 1200; the outer cylinder Reynolds number (Re_o) was fixed at 900. Based on the studies of Anderek et al.,[14] we judged the flow field in our study to be nonwavy axisymmetric Couette flow.

Table 1 Rotation rates for the Couette-flow bioreactor

Trial	Inner-cylinder speed ω_i, rpm	Outer-cylinder speed ω_o, rpm	Differential rate $\Delta\omega$, rpm
1	24	18	6
2	30	18	12
3	36	18	18

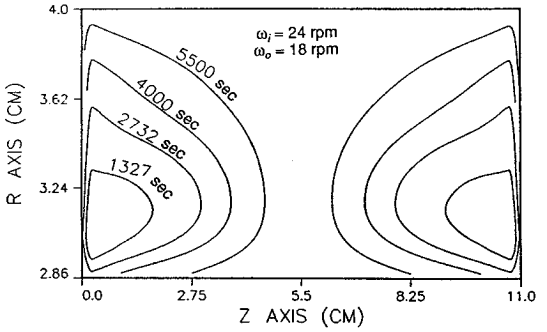

Fig. 3 Streamlines in the (r, z) plane and circulation times for trial 1.

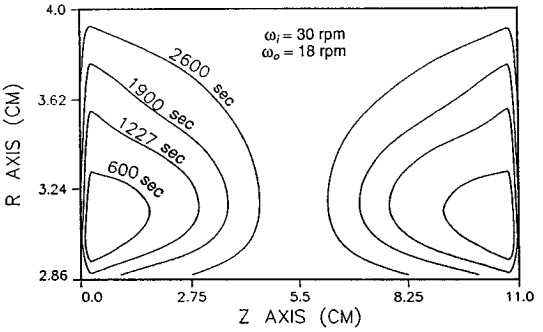

Fig. 4 Streamlines in the (r, z) plane and circulation times for trial 2.

We assumed that one continuous fluid phase would always be present, with particles suspended within the fluid. Therefore, the computational approach to this problem was to solve a system of partial differential equations, Eqs. (1–4), for the steady-state flowfield of the fluid, and then to solve the system of ordinary differential equations, Eqs. (5–7), for tracking representative particles. For Eqs. (1–4) a staggered discrete grid for the velocity components was used in a semi-implicit finite-difference algorithm employing a hybrid scheme developed by Spalding.[15–17] The grid has 61 subdivisions in the z direction and 10 subdivisions in the r direction. Since the flow was axially symmetric, flowfields were projected into the rectangular region of the (r, z) plane. Bilinear interpolation was used to approximate the complete steady-state flowfield throughout the region. Equations (5–7) were solved for the trajectories given the steady-state values of (u, v, w). The initial-value problem was a two-time-scale, three-dimensional, second-order system of ordinary differential equations. Both time scales came from the large difference between the rate of rotation and the rate of circulation in the secondary flow. The fast time scale, for the rotation of the vessel at approximately 20 rpm, was on the order of seconds, while the slow time scale, for the circulation of the flow, was on the order of minutes to hours. As a two-time-scale problem, Eqs. (5–7) gave a stiff system of ordinary differential equations with a 6×6 Jacobian matrix having at least two large eigenvalues and at least two small eigenvalues, requiring Gear's stiff method for trajectory calculations.

Simulation Results

Figures 3–5 illustrate segments of the secondary flowfields from the three trials. Printed along each streamline is the circulation time in seconds computed for the segment plotted in the (r, z) plane. At

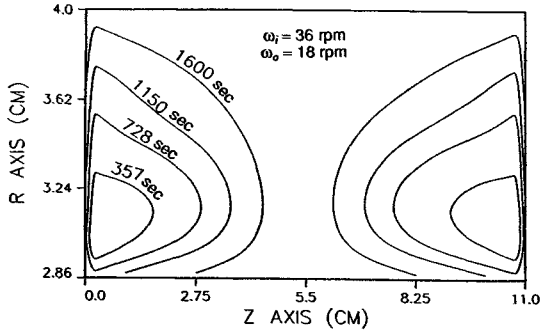

Fig. 5 Streamlines in the (r, z) plane and circulation times for trial 3.

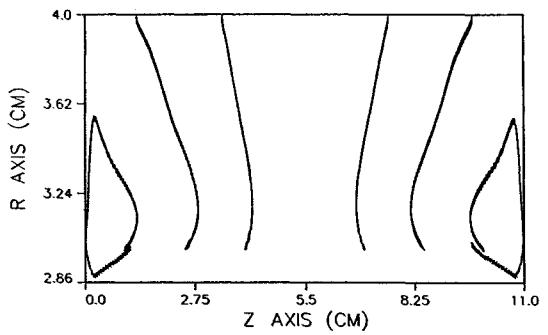

Fig. 6 Trajectories in the (r, z) plane for trial 1 at unit gravity.

the end vessel walls, viscous force slows the flow velocity, and the force due to the pressure gradient drives the flow inward to form the secondary flow. The circulation is two-compartmental, with counterclockwise flow in the left half and clockwise flow in the right half. A Runge-Kutta-Fehlberg numerical method[16] was used to generate the streamlines. However, the zero boundary conditions along the vessel walls, and the limitations in numerical accuracy due to the linear interpolation of the data for the flowfield, prevented the complete circulation from being plotted along streamlines near the end walls of the vessel. In these narrow regions, circulation was very slow, since u and w are close to zero. Figures 3–5 indicate that circulation may be poor in the middle of the vessel. For instance, results from trial 1 show a circulation time approximately 2 h; increasing the rotation speed in trial 3 decreased the circulation time to approximately 25 min. Higher differential rates of rotation created a stronger secondary flow; more studies are needed to determine if these circulation times impose significant mass-transfer limitations on distributing nutrients to the cells.

For each of the three trials, six trajectories were plotted in Figs. 6–8 at unit gravity ($g = 980$ cm/s^2) and in Figs. 9–11 at low gravity ($g = 0.0980$ cm/s^2), which was a reasonable assumption for the Space Shuttle flight environment. The initial conditions for these six trajectories were $r = 3$ cm, $\theta = 0$, $z = 1, 2.5, 4, 7, 8.5$, and 10 cm, with all first derivatives initially equal to zero. These figures demonstrate that a particle does not follow the streamlines precisely, but instead it migrates across streamlines. If a particle was within a region of strong circulation, then it completed its own cycle and remained suspended in the fluid. However, in most regions of the vessel a particle hit either the outer cylinder wall or an end wall. Computation of a trajectory was terminated when a particle either completed one cycle or hit a vessel wall. In trial 1, particles required more than 20 min to migrate to a vessel wall; in trial 3, by contrast, the time was reduced to less than 13 min. There was no appreciable difference in circulation time between unit gravity and microgravity. Thus, higher differential rotational rates provide stronger circulation and seem to increase the frequency of interactions between the particles and the vessel walls. Significant cellular damage was attributed to the impact of cells on the vessel wall, based upon observations of actual cell culture conditions. Quantitative evaluation of damage from wall collisions and resulting particle trajectories has yet to be performed.

The most noticeable difference between trajectories in unit gravity and microgravity was the presence (Figs. 6–8) of the significant

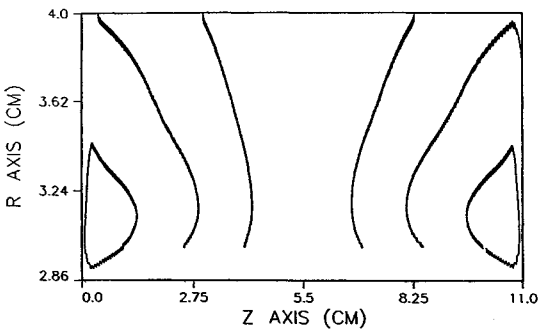

Fig. 7 Trajectories in the (r, z) plane for trial 2 at unit gravity.

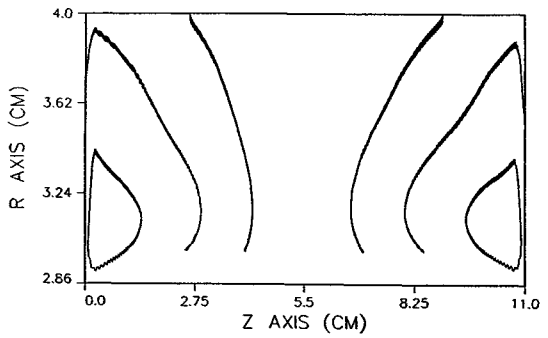

Fig. 8 Trajectories in the (r, z) plane for trial 3 at unit gravity.

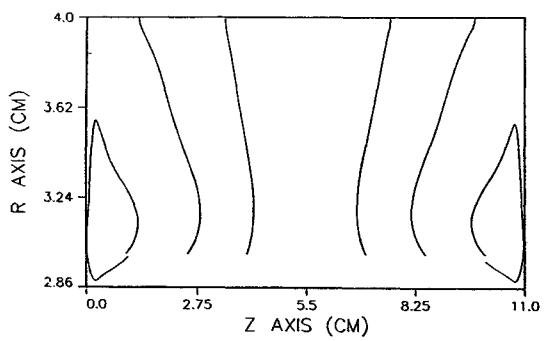

Fig. 9 Trajectories in the (r, z) plane for trial 1 at microgravity.

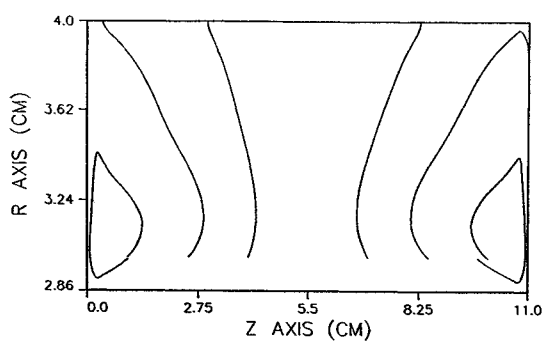

Fig. 10 Trajectories in the (r, z) plane for trial 2 at microgravity.

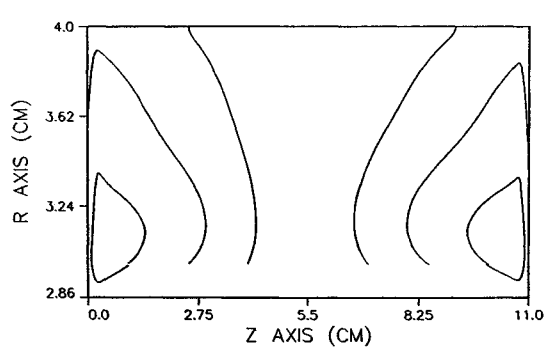

Fig. 11 Trajectories in the (r, z) plane for trial 3 at microgravity.

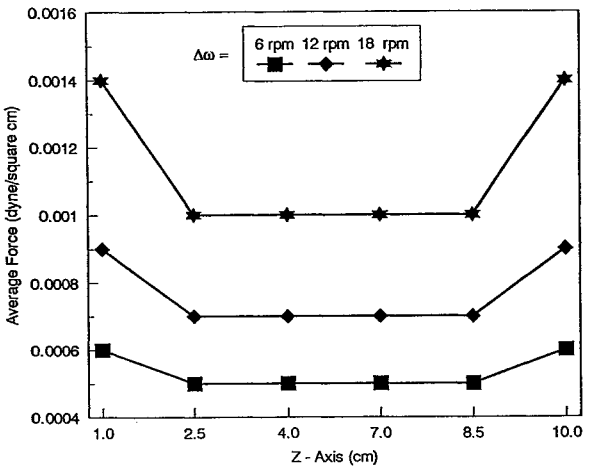

Fig. 12 Average force acting on a particle at unit gravity.

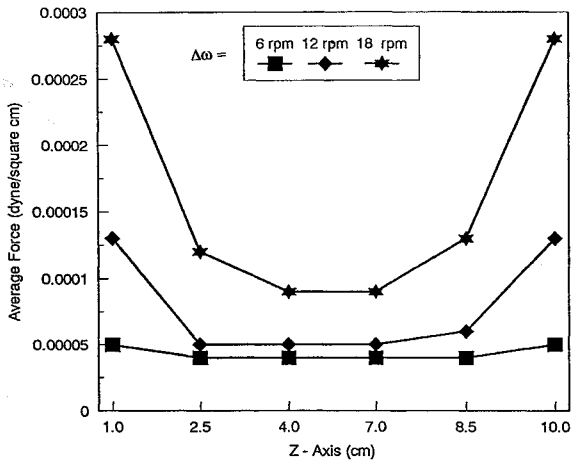

Fig. 13 Average force acting on a particle at microgravity.

gravity-induced particle oscillations in unit gravity, as previously described by Wolf and Schwarz.[11] The oscillations give the particles the appearance of tumbling, occurring once for every revolution of the vessel and having amplitudes on the order of 0.02 cm, depending on particle sedimentation rate, vessel rotation rate, and gravitational strength. Intuitively, one can speculate that the oscillations represent a deviation in the trajectory as a direct result of unit-gravity sedimentation and may cause the boundary-layer separation along particles. This gravity-induced motion is therefore a prime justification for development of improved microgravity culture techniques in which this effect is absent. The utility of dynamic modeling is in the ability to calculate the total force on a particle as a function of time. In this study, the total force per unit of cross-sectional area on a particle was computed in real time by calculating the vector sum of the forces in Eqs. (5–7) divided by the cross-sectional area, $\pi d^2/4$, of a particle. The time-average values of the total force are plotted in Figs. 12 and 13 for the six trajectories in each of the three trials at both unit gravity and microgravity. The average force ranged from 0.0005 to 0.0014 dyne/cm^2 in unit gravity and from 0.00004 to 0.00028 dyne/cm^2 in microgravity. These values were significantly less than that anticipated by the analysis of hydrodynamic forces. In general, the force on a particle in microgravity was one order of magnitude smaller than that in unit gravity.

Experimental Verification

The numerical model was verified experimentally in the space environment. In order to increase the cell-culture capacity and optimize the flowfield, we used a 500-ml vessel in the study. The only deviation from the vessel used in numerical simulation was that the inner-cylinder radius was changed to 1.25 cm. We kept very slow rotation, such that Re_i ranged from 190 to 490 and Re_o from 240 to 1560. The flowfield in this space experiment was azimuthal laminar flow with weak Ekman vortices.[14] The bioreactor was flown on Space Shuttle Atlantis in November 1991. The experimental apparatus, shown in Fig. 14, consisted of one module divided into two sections: one with the reactor vessel, fluid-filled components, light, and vessel drive motors, and the other with camera, tape supply, control electronics, and power supply. The fluid used was water rather than liquid-cell culture media, and small beads served as cell aggregates. The experiment included 16 different sequences based on the rotating speeds of the inner and outer cylinders and perfusion loop. Table 2 shows the setup of experiment protocols.

The flight data verified that sequences 1 and 2 produced optimal operating conditions. In sequence 1, the outer wall was rotated at 2 rpm and the inner wall at 6 rpm. Video images showed that at startup the beads were congregated on the outer wall. After about an hour, the small beads (1000 μm) were trapped by the flowfield in the left half of the vessel and were well distributed from the inner wall to the outer wall. The medium beads (3000 μm) were uniformly distributed in both halves of the vessel. The large beads (5000 μm) were positioned near the end caps and closer to the inner wall. The rotation rates in sequence 2 were the same as those in sequence 1; however, a perfusion rate of 20 cm^3/min was established. The old medium was removed from the center of the inner cylinder and fresh medium injected from both ends. The small and medium beads were closer to the inner wall, and the large beads moved farther away from the end caps.

Table 2 Bioreactor sequence chart and particle suspension results for the space-flight experiment[a]

Sequence	Outer speed, rpm	Inner speed, rpm	Pump rate,[b] cm^3/min	Results[c]
1	2	6	0	S^1
2	2	6	20	S^1
3	5	5	0	O
4	5	5	20	O
5	5	7	0	O
6	5	7	20	O
7	5	9	0	O
8	5	9	20	O
9	5	13	0	S^2
10	5	13	20	S^2
11	13	5	0	O
12	13	5	20	O
13	9	5	0	O
14	9	5	20	O
15	7	5	0	O
16	7	5	20	O

[a]Space Shuttle middeck experiment DSO-316 on STS-44.
[b]The medium comes in from the both ends of the inner cylinder and extracts out from the middle of the same cylinder.
[c]S^1: suspension of all particles achieved; S^2: suspension of 1000-μm particles achieved; O: all particles move to the outer cylinder.

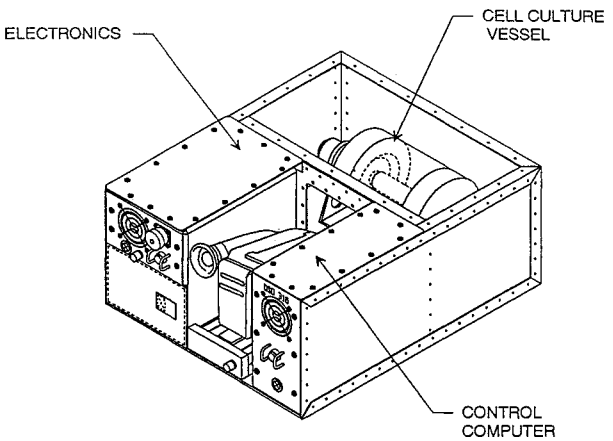

Fig. 14 Flight hardware of DSO-316 with rear cover removed.

Table 3 Comparison of predicted and observed axial (z-direction) migration of particles in sequence 1 of space-flight experiment

Particle size μm	Speed, mm/s	
	Predicted	Observed
1000	0.014	0.039
3000	0.016	0.044
5000	0.020	0.075

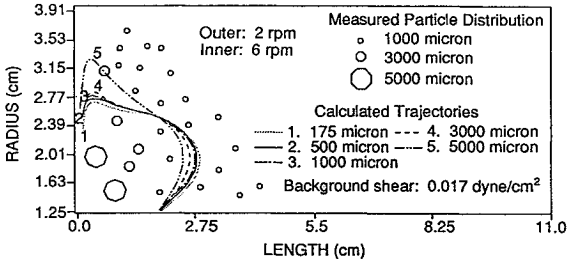

Fig. 15 Comparison of observed particle distributions and numerical simulations.

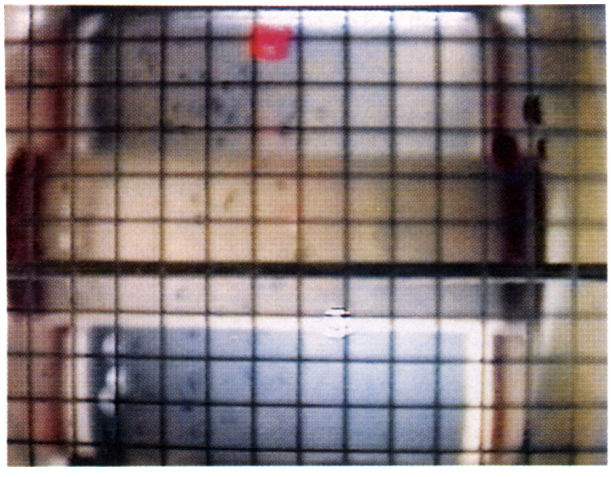

Fig. 16 Video recording of sequence 1 in microgravity experiment.

Figure 15 shows an overlay of the observed particle distributions from the analysis of the continuous video images and the predicted trajectories based on the three particle sizes as described. There was one video camera mounted in the DSO 316 experiment; the recordings only showed the two-dimensional distribution of particles. Figure 16 shows a freeze frame of particles distribution in the experiment. The results of simulations showed that the secondary flow was strong enough to force particles to assume curved trajectories and undergo a circular motion with circulation time of 25 ± 5 min. The distribution from the flight data showed that when particles hit the end cap, only the 1000-μm particles could be swept away by the fluid circulation. The larger particles were too heavy to be dragged away by the fluid's inward circulation and stayed near the surface of the inner spin cylinder.

We measured the migration of particles along the z axis; Table 3 shows a comparison between the observed and the predicted migration velocity for different sizes of particles. When the perfusion was turned on, the particles were brought in toward the inner wall, and the 5000-μm particles were moved outward by the circulation force. Sequences 9 and 10 also indicated that partial suspension of particles (1000 μm) was achieved. The secondary flow was not strong enough to overcome the centrifugal effect (outer cylinder rotated at 5 rpm) for larger particles. Sequences 3 to 8, with the inner cylinder rotated faster than the outer cylinder, showed that the centrifugal force was too strong; all particles were sent towards the outer wall eventually. These flight data were in good agreement with the calculated trajectories from the model (Fig. 17). Sequences 11 to 16, with the outer cylinder rotated faster than the inner cylinder, showed

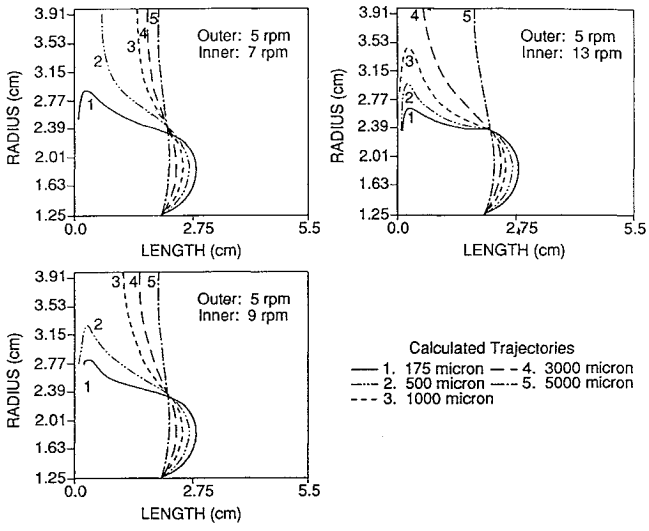

Fig. 17 Numerical simulation of particle trajectories for sequences 5, 7, 9 in space-flight experiment.

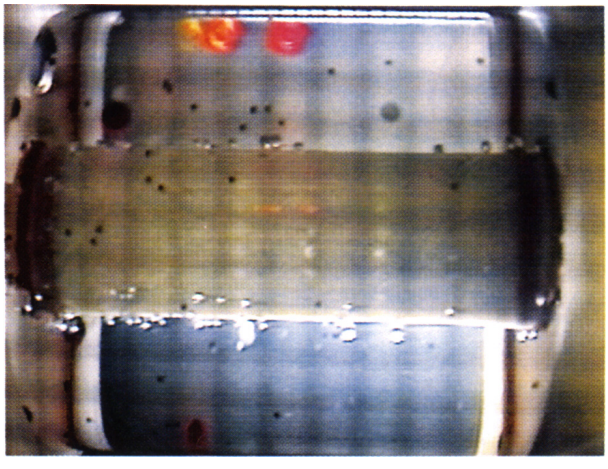

Fig. 18 Video recording of sequence 13 in microgravity experiment.

that all particles were sent towards the outer wall due to the dominant centrifugal force, but we observed some 1000-μm particles attached to the inner cylinder (Fig. 18), which may cause clogging of the perfusion mechanism.

A small bubble was observed at the initiation of the experiment. The number of bubbles increased as the experiment progressed. The bubbles were primarily positioned around the inner wall, mainly due to centrifugal force. We also observed that some of the beads, regardless of size, were captured by the bubbles and held by surface tension. The largest bubble was about 5 ml and was located against the left-side end cap. The exact source of the bubbles has yet to be determined. The flight data indicate the following findings:

1) The range of inner vs outer rotation speeds resulting in cell suspension is consistent with the mathematical model.

2) The axial migration of particles in the reactor vessel is approximately 3 times bigger than the mathematical model predicts, due to modeling inaccuracies.

3) Experiments suggest that counterrotating cylinders do not suspend particles, except for some small particles which seem to be caught in a local low-pressure region near the inner cylinder.

Conclusions

Mathematical models of the rotating bioreactors designed at Johnson Space Center were developed to partially simulate microgravity with respect to the trajectories and time frame of a slowly sedimenting particle's motion. Except for a gravity-induced oscillation on each revolution, a particle in unit gravity will follow the same primary trajectory as a particle in space, even though the strengths of the dominant forces controlling the dynamics are quite different.

Although microcarrier beads can be suspended without turbulence in these rotating bioreactors on Earth, the advantage of operating the bioreactor in space is the significant reduction of total force on a particle through eliminating the g-induced oscillatory particle motion. This motion is the primary cause of residual shear stress in the rotating culture vessels operated in unit gravity. The total force on a particle in this study was less than the values reported by other investigators using different vessel geometries to model hydrodynamic effects on cell growth. The hydrodynamic conditions in the Couette bioreactor are well defined and nonturbulent, making it a good choice for studies relating hydrodynamics to cell or tissue-culture performance. The tumbling effect may facilitate energy dissipation by the particle, leading to a force per unit cross-sectional area on a particle that is less than the analysis of hydrodynamic forces would indicate. In either unit gravity or space, the greatest potential for cell damage occurs when the particle is near the vessel wall or collides with the wall.

Increasing the differential rate of rotation in this study strengthened the secondary flow but did not seem to entrap particles within the flow. Faster rotation decreased the time between impacts with the vessel walls, thereby increasing the number of collisions. A larger gap between the inner and outer cylinders would decrease the number of collisions, but would weaken the circulation of the fluid from the secondary flow. Further study is needed to determine optimal design and optimal rates of rotation to minimize particle collisions with the outside wall and end caps due to the stronger secondary flow while still providing adequate circulation for mass transfer of nutrients and removal of cellular waste products.

Acknowledgment

Support for Dr. Boyd was provided by the Office of Space Science and Applications through the NASA JOVE Program.

References

[1]Fiechter, A., "Process Development for Hybridoma Cells," *Advances in Biochemical Engineering/Biotechnology*, Vol. 37, Springer-Verlag, Berlin, 1988, pp. 35–38.

[2]Pollard, E. C., "Theoretical Studies on Living Systems in Absence of Mechanical Stress," *Journal of Theoretical Biology*, Vol. 8, No. 1, 1965, pp. 113–123.

[3]Moroz, P. E., "The Cell in the Field of Gravity and the Centrifugal Field," *Journal of Theoretical Biology*, Vol. 107, No. 2, 1984, pp. 303–320.

[4]Stathopoulos, N. A., and Hellums, J. D., "Shear Stress Effects on Human Embryonic Kidney Cells in Vitro," *Biotechnology and Bioengineering*, Vol. 27, July 1985, pp. 1021–1026.

[5]Croughan, M. S., Hamel, J. F., and Wang, D. I. C., "Hydrodynamic Effects on Animal Cells Grown in Microcarrier Cultures," *Biotechnology and Bioengineering*, Vol. 29, Jan. 1987, pp. 130–141.

[6]Croughan, M. S., and Wang, D. I. C., "Growth and Death in Overagitated Microcarrier Cell Cultures," *Biotechnology and Bioengineering*, Vol. 33, Feb. 1989, pp. 731–744.

[7]Cherry, R. S., and Papoutsakis, E. T., "Hydrodynamic Effects on Cells in Agitated Tissue Culture Reactors," *Bioprocess Engineering*, Vol. 1, 1986, pp. 29–41.

[8]Cherry, R. S., and Papoutsakis, E. T., "Physical Mechanisms of Cell Damage in Microcarrier Cell Culture Bioreactors," *Biotechnology and Bioengineering*, Vol. 32, Oct. 1988, pp. 1001–1014.

[9]Tsao, Y. D., Goodwin, T. J., Wolf, D. A., and Spaulding, G. F., "Responses of Gravity Level Variations on the NASA/JSC Bioreactor System," *The Physiologist*, Vol. 35, No. 1, 1992, pp. 49, 50.

[10]Schwarz, R. P., Goodwin, T. J., and Wolf, D. A., "Cell Culture for Three-Dimensional Modeling in Rotating-Wall Vessels: Applications of Simulated Microgravity," *Journal of Tissue Culture Methods*, Vol. 14, No. 1, 1992, pp. 51–58.

[11]Wolf, D. A., and Schwarz, R. P., "Analysis of Gravity-Induced Particle Motion and Fluid Perfusion Flow in the NASA-Designed Rotating Zero-Headspace Tissue Culture Vessel," NASA Technical Paper TP-3143, Oct. 1991.

[12]Bird, R. B., Stewart, W. E., and Lightfoot, E. N., *Transport Phenomena*, Wiley, New York, 1960, pp. 83–91.

[13]Bird, R. B., Stewart, W. E., and Lightfoot, E. N., *Transport Phenomena*, Wiley, New York, 1960, pp. 132, 133.

[14]Andereck, C. D., Liu, S. S., and Swinney, H. L., "Flow Regimes in a Circular Couette System with Independently Rotating Cylinders," *Journal of Fluid Mechanics*, Vol. 164, No. 6, 1986, pp. 155–183.

[15]Patankar, S. V., and Spalding, D. B., "A Calculation Procedure for Heat, Mass and Momentum Transfer in Three Dimensional Parabolic Flows," *International Journal of Heat and Mass Transfer*, Vol. 15, 1972, p. 1987.

[16]Patankar, S. V., *Numerical Heat Transfer and Fluid Flow*, McGraw-Hill, New York, 1980, p. 197.

[17]Hung, R. J., Tsao, Y. D., Hong, B. B., and Leslie, F. W., "Dynamical Behavior of Surface Tension on Rotating Fluids in Low and Microgravity Environments," *Applied Microgravity Technology*, Vol. 2, No. 2, 1989, pp. 81–95.